Eur. Phys. J. C 52, 759–764 (2007)
DOI 10.1140/epjc/s10052-007-0431-3

THE EUROPEAN PHYSICAL JOURNAL C

Special Article – Tools for Experiment and Theory

Refractive index dispersion law of silica aerogel

T. Bellunato[a], M. Calvi, C. Matteuzzi, M. Musy, D.L. Perego, B. Storaci

Università degli Studi di Milano Bicocca and INFN, Piazza della Scienza 3, 20126 Milano, Italy

Received: 31 July 2007 / Revised version: 7 September 2007 /
Published online: 26 September 2007 –

Abstract. This paper presents measurements of the refractive index of a hygroscopic silica aerogel block at several wavelengths. The measurements, performed with a monochromator, have been compared with different parameterisations for $n(\lambda)$, in order to determine the best chromaticity law for the aerogel. This is an important input for design and operation of RICH detectors with silica aerogel radiator.

PACS. 29.40.Ka; 78.20.Ci

1 Introduction

Silica aerogel has gained in the last decade a prominent role in high energy physics as a radiator for Ring Imaging Cherenkov (RICH) detectors. Its refractive index, tunable at the production stage in the range 1.01–1.1, makes it a suitable tool for the identification of charged particles from 1 GeV/c to a few GeV/c in momentum.

The refractive index of a dielectric material is wavelength dependent. The dependence of the refractive index of a dielectric medium on the photon wavelength, the so-called dispersion law or chromaticity $n = n(\lambda)$, is related to the reconstructed angle θ_C by the Cherenkov relation [1]:

$$\theta_C = \arccos\left[\frac{1}{n(\lambda)\beta}\right]. \quad (1)$$

The resolution of a RICH detector is intrinsically limited by the chromatic dispersion of its radiator [2]. Therefore it is important to know the dispersion law both for simulation and for reconstruction purposes.

Silica aerogel, produced by the Boreskov Institute of Catalysis (Novosibirsk) with a refractive index $n \sim 1.03$ has been produced for the LHCb RICH detector [3–6]. This aerogel is hygroscopic and several tests have been already performed during the R&D phase on its optical properties, ageing and performances [7, 8].

Since most photon detectors work in the wavelength range 200–700 nm, the behaviour of the index of refraction within this range is the subject of this paper.

2 The refractive index

A common way to measure the refractive index n of a dielectric solid material like silica aerogel is the prism method which is shown in Fig. 1. Assuming the index of refraction of air $n_{air} = 1$, simple calculations in the classical geometrical optics framework give the following formula:

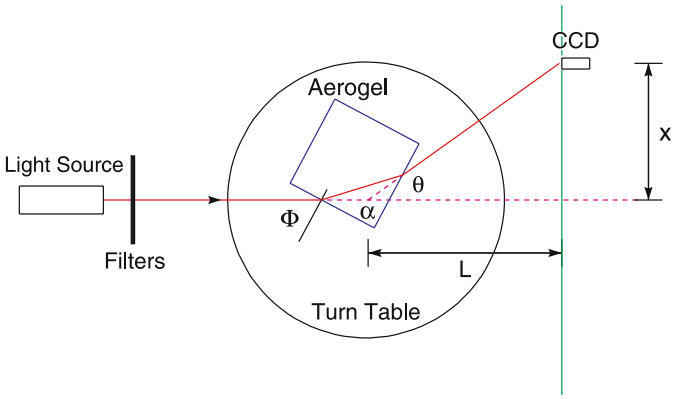

Fig. 1. Set–up of the prism method measurement of the silica aerogel refractive index n

$$\theta = \Phi + \arcsin\left\{n \sin\left[\alpha - \arcsin\left(\frac{\sin\Phi}{n}\right)\right]\right\} - \alpha\,. \quad (2)$$

Here, θ is the deflection angle, Φ is the incident angle on the aerogel surface, n is the refractive index of the solid and α is the angle between the two adjacent sides of the block. The measurements described in the following sections have been performed on an aerogel sample precisely cut and polished after the production, with $\alpha = 90° \pm 0.1°$. In the minimum deviation condition, (2) becomes:

$$n = \frac{\sin\left(\frac{\alpha+\theta}{2}\right)}{\sin\left(\frac{\alpha}{2}\right)}\,. \quad (3)$$

[a] e-mail: tito.bellunato@cern.ch

The dispersion law of aerogel can be parameterised in several ways. The Lorentz–Lorenz dispersion law [1] is given by:

$$\frac{n^2-1}{n^2+2} = cf(E_\gamma)\,, \quad \text{with} \quad c = \frac{4\pi a_0^3 \rho N_\mathrm{A}}{3M}\,, \tag{4}$$

being a_0 the Bohr radius, ρ the density of the medium, M its molecular weight and N_A is the Avogadro constant. The energy dependence of the molar refractivity $f(E_\gamma)$ can be parameterised in terms of a multi-pole Sellmeier function as:

$$f(E) = \sum_{j=1}^{N} \frac{F_j}{E_j^2 - E_\gamma^2}\,, \tag{5}$$

where F_j and E_j are the Sellmeier coefficients and N is the number of poles to be used to fit data. Equation (5) can be written as a function of wavelengths. One- and two-pole approximations for the dependence as a function of λ are:

$$n^2(\lambda) - 1 = \frac{a_0\lambda^2}{\lambda^2 - \lambda_0^2}\,, \tag{6}$$

$$n^2(\lambda) - 1 = \frac{a_1\lambda^2}{\lambda^2 - \lambda_1^2} + \frac{a_2\lambda^2}{\lambda^2 - \lambda_2^2}\,. \tag{7}$$

A two-pole Sellmeier heuristic formula that parameterises the refractive index as a function of the energy E_γ of the incident photon is often found in literature.

3 The experimental set-up

Refractive indices at several wavelengths have been measured using the experimental arrangement shown in Fig. 1. A monochromator[1] coupled to a Xe-UV lamp has been used as light source. It selects wavelengths from 200 nm to 900 nm, with a resolution of 1 nm.

The deflection angle was determined by measuring the displacement x with a CCD camera[2] located at a distance $L = 47.5$ cm from the aerogel. The camera is fixed to a support sliding on a rail transversely with respect to the light beam to allow the positioning of the spot inside the CCD sensor. The fine measurement of the deflection was performed calculating the centre of gravity of the beam spot image on the sensor with a typical resolution of the order of 20 μm. Typically, the light deviation x was about 3 cm in the plane containing the CCD sensor.

To obtain a better defined spot on the CCD display, measurements were performed at a generic fixed incident angle Φ and not at the minimum deviation position. With this configuration the refractive index n has been evaluated by solving numerically equation (2).

[1] Jobin Yvon Horiba H10, 1200 g/mm grating.

[2] SONY® XC-ST70CE with 768×512 pixels and a sensitive area of 1.025×0.850 cm^2.

4 Results

A precise measurement of the incident angle Φ was not possible; its value has been estimated by (2) as the value giving $n = 1.0283$ at $\lambda = 632.8$ nm, as previously determined with the minimum deviation method using a He-Ne laser as light source.

For each selected wavelength λ, the value of the refractive index $n(\lambda)$ has been obtained from (2).

The evaluation of the uncertainty in the measurement of the refractive index, σ_n, has been performed using a Monte Carlo simulation in which all variables in (2) are normally distributed around their measured values. The standard deviation of each distribution is assumed as the experimental uncertainty on each variable. Local small flatness variations mimic deviations of α from right angle, therefore they are implicitly taken into account in the simulation.

The Φ uncertainty is the same for all the experimental data so that it is considered as a correlated error and its contribution to the refractive index uncertainty σ_n has been considered separately as explained at the end of this section.

Data have been fitted with (6). The data and the fit function are shown in Fig. 2. The results for the two parameters a_0 and λ_0 are shown in Table 1. An attempt to fit experimental data with a two-pole Sellmeier formula in the range 350–700 nm gives two superimposed poles showing that there is no sensitivity to discriminate the second pole.

Aerogel is a mixture of air, silica particles and some residual impurities such as water and ethanol. As a first approximation it can be considered as a less dense form of fused silica. In order to verify this hypothesis, the constants a_0 and λ_0 from aerogel have been compared to those from quartz [9]. Data are listed in Table 1. The pole found for the aerogel is close to the pole of the pure fused silica. However, since in our case the pole is shifted towards shorter wavelengths, in the wavelength range investigated the dispersion curve is less steep than the one resulting from a pedestrian application of the Lorentz–Lorenz law to fused silica data. This, in turn, results in a smaller chromatic dispersion.

In the pure fused silica model, the a_0 parameter is related to the density of the material. Under this approximation, using (4) it is possible to calculate the density of the aerogel tile from the relation:

$$\rho(\text{aerogel}) = \frac{a_0(\text{aerogel})}{a_0(\text{SiO}_2)} \frac{n^2(\text{SiO}_2)+2}{n^2(\text{aerogel})+2} \rho(\text{SiO}_2)\,. \tag{8}$$

For the parameters listed in Table 1 one can determine a density $\rho(\text{aerogel}) = (0.158 \pm 0.001)$ g/cm^3. This value is in coarse agreement with $\rho_0 = (0.149 \pm 0.004)$ g/cm^3 provided by the manufacturer. Therefore, it is possible to consider, for our purposes, that aerogel is a binary mixture of pure fused silica and air with a one-pole dispersion law in the range 350–700 nm.

A comparison with a similar measurement performed on a hydrophobic aerogel tile has also been done. In this

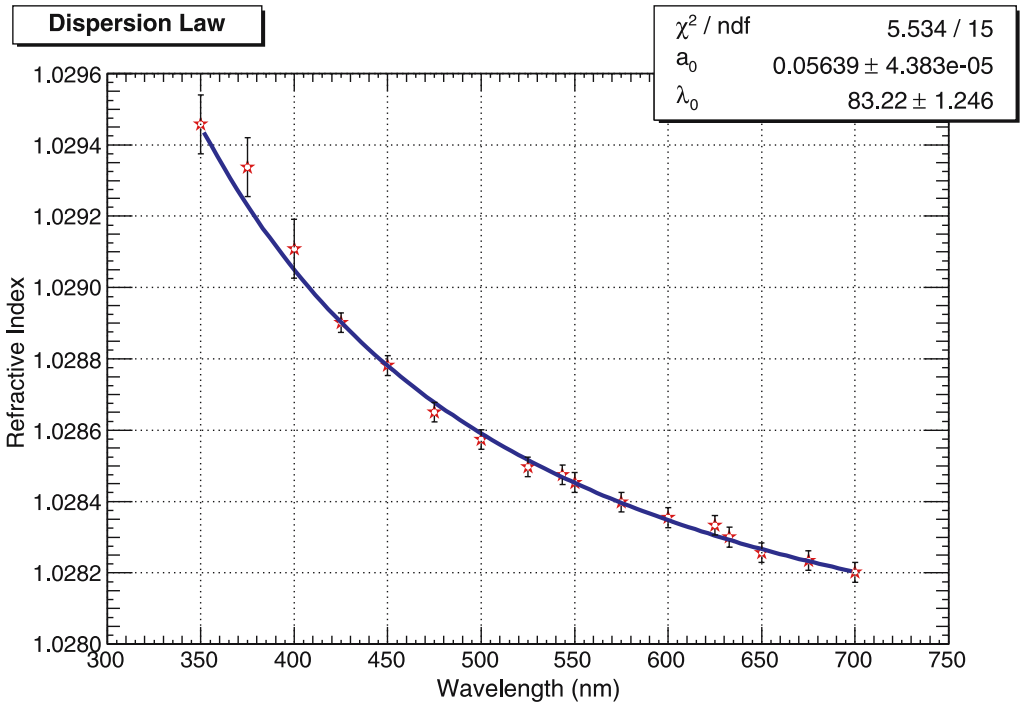

Fig. 2. Chromatic dispersion $n = n(\lambda)$ measured in a hygroscopic silica aerogel tile. A one-pole Sellmeier parameterisation has been fitted to experimental data

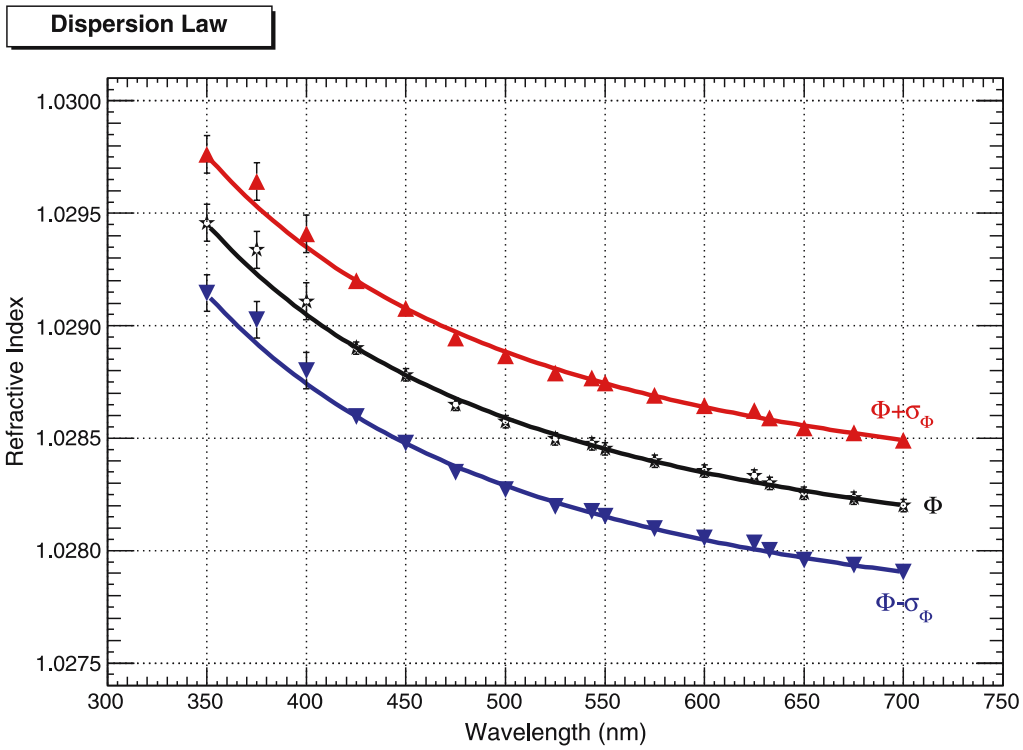

Fig. 3. Experimental data obtained with Φ, $\Phi + \sigma_\Phi$ and $\Phi - \sigma_\Phi$ and fitted to the one-pole Sellmeier formula

Table 1. Parameters of one-pole Sellmeier equation for aerogel from fit and for pure fused silica from [9]

	Aerogel	Pure fused silica
a_0	0.05639 ± 0.00004	1.0963 ± 0.00002
λ_0 (nm)	83.22 ± 1.25	93.76 ± 0.01

case, $a_0 = (0.0536 \pm 0.0003)$ and $\lambda_0 = (91.82 \pm 3.82)$ nm have been measured [10]. As before, the pole position is directly comparable with the one from the hygroscopic aerogel, while the a_0 coefficient cannot because this parameter is density-dependent. This comparison indicates to a 2σ level that the dispersion curve is flatter for hygroscopic aerogel in the wavelength range 350–700 nm.

Table 2. Results of the fit with one-pole Sellmeier formula for different input values of Φ

	a_0	λ_0 (nm)
$\Phi - \sigma_\Phi$	0.05579 ± 0.00003	83.15 ± 0.95
Φ	0.05639 ± 0.00004	83.22 ± 1.25
$\Phi + \sigma_\Phi$	0.05698 ± 0.00004	83.29 ± 1.25

The uncertainty on the entrance angle, $\sigma_\Phi = 8$ mrad, has been determined from the measurement of the refractive index at $\lambda = 632.8$ nm with the laser. To evaluate the effect of σ_Φ, the aerogel refractive index has been determined using the reference value $\Phi = 536$ mrad and $\Phi \pm \sigma_\Phi$.

The three datasets $(\lambda, n(\lambda))$ have been then fitted with (6). Results are shown in Fig. 3 and Table 2. The variation of Φ produces a shift, but the shape is not affected. The effect on λ_0 is masked by its uncertainty, but the a_0 scaling parameter is slightly different in the three cases. So the uncertainty on Φ mimics a density effect. Our determination of the parameter is $a_0 = (0.05639 \pm 0.00004 \pm 0.0006)$ where the statistical error is the first term while the systematic part is given by the second term.

5 Particle identification and chromaticity

The effects of the dispersion law of the aerogel on the particle identification performances in a RICH detector have been investigated with a dedicated simulation. The GEANT4 toolkit has been used [11]. An existing simulation package used to study the refractive index inhomogeneity, described in detail elsewhere [8], has been adapted to the current scope.

The inputs to the simulation are the optical properties of the aerogel tile and its size, $200 \times 200 \times 50\,\mathrm{mm}^3$. The program then generates a bunch of charged particles which traverse the aerogel perpendicular to the wider surfaces. The Cherenkov photons produced in the aerogel are traced along their path, can undergo Rayleigh scattering and are focused by a tilted spherical mirror ($R = 949$ mm) onto a photon detector whose quantum efficiency has been set to be the same as for the LHCb photon detectors [12].

Mixtures of K^- and π^- beam (60 k particles in total for each run) with a momentum of 10 GeV/c have been generated. Four different parameterisations of the dispersion law of the aerogel have been used:

1. $n_1 = \mathrm{const}$, wavelength-independent;
2. $n_2 = n_2(\lambda)$, the one-pole Sellmeier formula measured in this paper;
3. $n_3 = n_3(\lambda)$ derived from the the Clausius–Mossotti equation assuming a simple binary mixture of air and SiO_2 [13];
4. $n_4 = n_4(\lambda)$, a two-pole Sellmeier formula used in the LHCb standard simulation [4].

The graph of these dispersion curves is shown in Fig. 4; the density dependent factors have been tuned so that the distributions match the value $n = 1.0283$ measured at $\lambda = 632.8$ nm.

A hit by hit reconstruction algorithm [14] allows one to build the distribution of the Cherenkov emission angle θ_C from the hits on the detection plane. The information used are the beam direction, the photon emission point, the position in space of the centre of curvature of the mirror

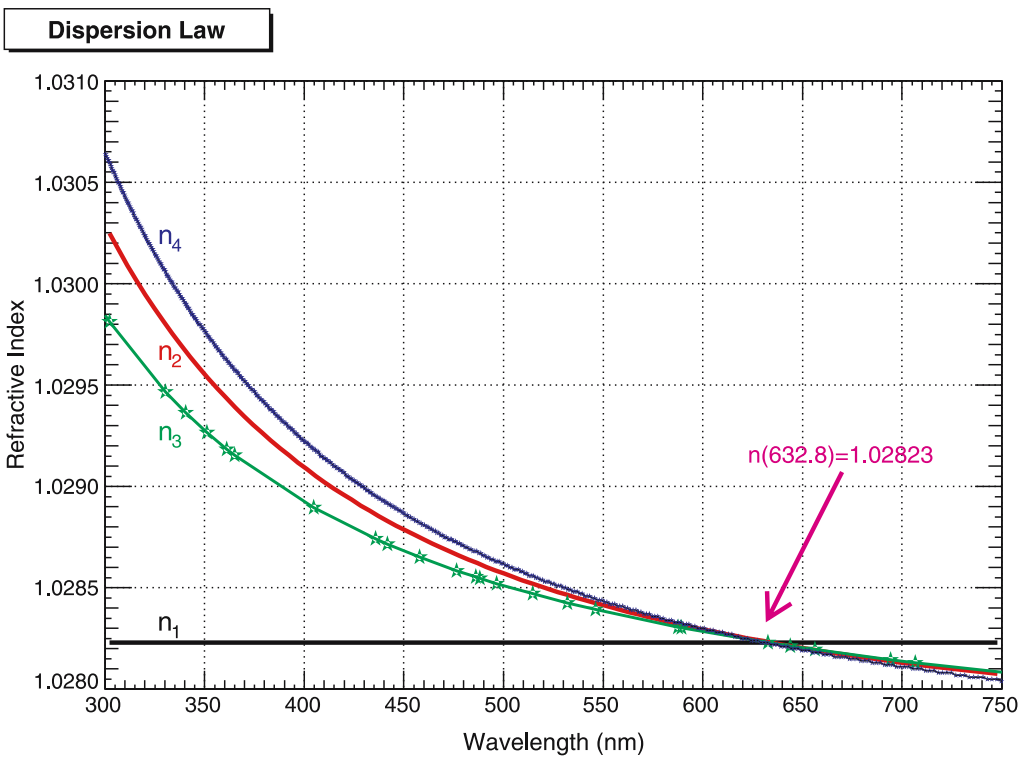

Fig. 4. Dispersion laws used in the simulation

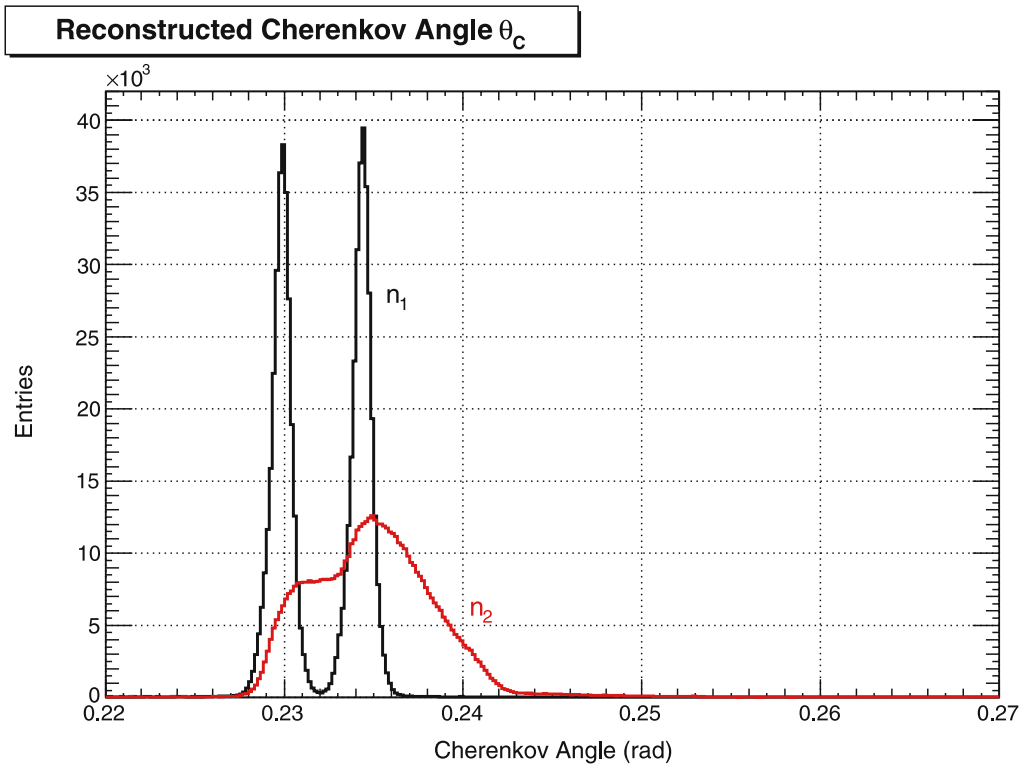

Fig. 5. Distributions of reconstructed θ_C from mixed K^- and π^- simulated beam with n_1 (*black*) and n_2 (*red*) runs

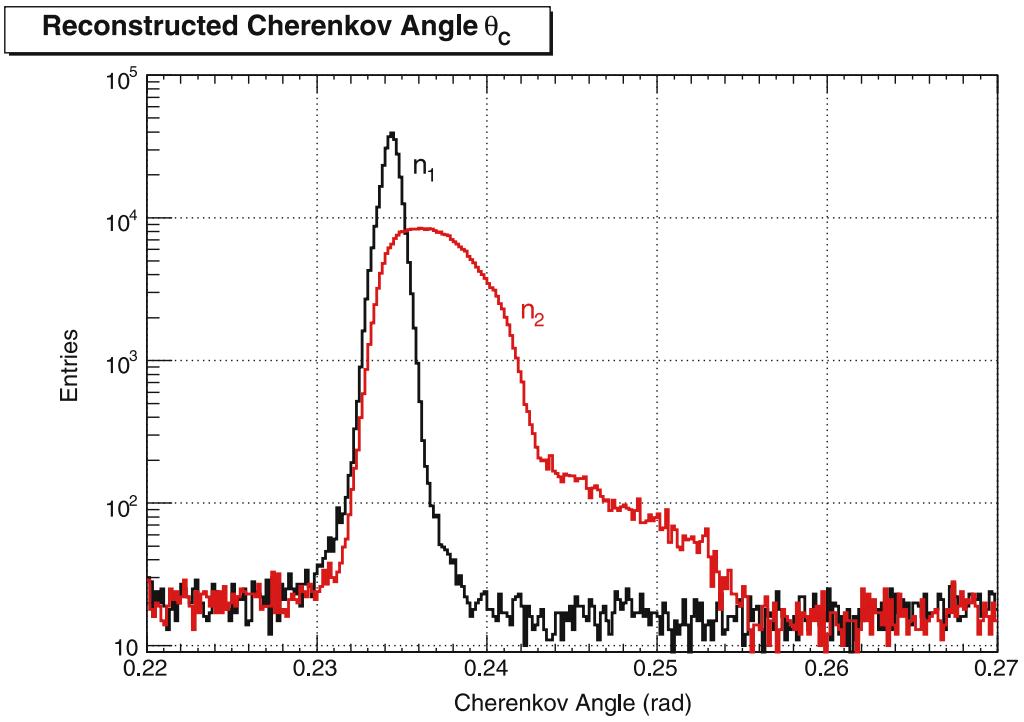

Fig. 6. Distributions of reconstructed θ_C from pure π^- simulated beam with n_1 (*black*) and n_2 (*red*) runs

and its radius. All the photons are assumed to be produced halfway inside the aerogel along the beam direction. In the reconstruction algorithm the information from the dispersion law is not used.

The reconstructed Cherenkov angle distributions are plotted in Fig. 5 for the first two cases n_1 and n_2. The distributions for n_3 and n_4 are similar to the n_2 case. The widths of the two peaks corresponding to pions and kaons in the $n_1 = \text{const}$ run are due to spherical aberration from the tilted mirror and the uncertainty on the emission point. In the $n_2(\lambda)$ run the chromaticity effects, modulated by the quantum efficiency of the photo-cathode, determine the blurred shape of the distribution. In Fig. 6 only the pion component is plotted.

Table 3. Mean Cherenkov angle θ_C and single photon resolution σ_θ (mrad) for the different dispersion laws and particle species considered in the simulation

	K^-		π^-	
	θ_C (mrad)	σ_θ (mrad)	θ_C (mrad)	σ_θ (mrad)
n_1	229.8	0.6	234.3	0.5
n_2	231.8	2.8	236.3	2.8
n_3	231.6	2.1	236.1	2.0
n_4	231.9	3.5	236.4	3.5

For each run and for each kind of particle, the average value of the reconstructed angle θ_C and the standard deviation of the single photon resolution have been determined with a gaussian fit. Results are listed in Table 3. When n is not constant in the simulation the widths of the two distributions are larger and the peaks are shifted with respect to the wavelength-independent case. The shift is of the order of 2 mrad. The mean θ_C values do not differ much for the different parameterisations, while the single photon resolutions differ substantially.

6 Conclusions

The resolution of a RICH detector is limited by the chromatic dispersion of its radiator. The refractive index $n(\lambda)$ in the wavelength range 350–700 nm has been measured using a monochromator and the prism method.

In this range the one-pole Sellmeier function is found to be a good approximation for the dispersion law. The parameters obtained for the aerogel are compared with the ones for pure fused silica. The pole for the aerogel is at shorter wavelengths with respect to fused silica, while the density-dependent parameter is found to be compatible with the properly scaled fused silica one.

Simulation studies show that different assumptions on the functional form of the dispersion law, although leading to the same average Cherenkov emission angle, imply substantially different single photon resolutions. The particle identification performance of a RICH detector strongly depends upon this parameter. The determination of the correct law therefore is a powerful tool in the conceptual design of an aerogel-based Cherenkov detector.

Acknowledgements. We gratefully acknowledge the skilled technical support of R. Mazza and the fruitful discussions with G. Lucchini about the experimental setup. We wish to thank G. Carboni (Università di Roma Tor Vergata) who has kindly provided part of the experimental equipment. Financial support from INTAS–5579 and HP–I3 contracts is acknowledged.

References

1. J.D. Jackson, Classical Electrodynamics (J. Wiley & Sons Inc., New York, 1999)
2. T. Ypsilantis et al., Nucl. Instrum. Methods A **343**, 30 (1994)
3. The LHCb Coll., LHCb Technical Proposal, CERN/LHCC/98-4 (1998)
4. The LHCb Coll., LHCb RICH Technical Design Report, CERN/LHCC/2000-037 (2000)
5. The LHCb Coll., LHCb Reoptimized Detector Design and Performance, CERN/LHCC/2003-030 (2003)
6. N. Brook et al., LHCb RICH 1 Engineering Design Review Report (LHCb 2004–121)
7. T. Bellunato et al., Nucl. Instrum. Methods A **527**, 319 (2004)
8. T. Bellunato et al., Nucl. Instrum. Methods A **556**, 140 (2006)
9. Melles Griot Inc., MELLES GRIOT Catalog – Optics Guide Vol. X (2007)
10. M.F. Villoro et al., Nucl. Instrum. Methods A **480**, 456 (2002)
11. A. Agostinelli et al., Nucl. Instrum. Methods A **506**, 250 (2003)
12. M. Moritz et al., IEEE Trans. Nucl. Sci. **51**, 1060 (2004)
13. G. Aglieri Rinella et al., Test-beam Results from a RICH Detector Prototype Using Aerogel Radiator and Pixel Hybrid Photon Detectors (LHCb 2006–006)
14. R. Forty, Nucl. Instrum. Methods A **384**, 167 (1996)